JGR Biogeosciences

RESEARCH ARTICLE
10.1029/2024JG008713

Special Collection:
Advancing Interpretable AI/ML Methods for Deeper Insights and Mechanistic Understanding in Earth Sciences: Beyond Predictive Capabilities

Key Points:
- Developed a new machine-learning based regression model to predict peat depths
- Generated a peat depth map over a very large area with a high resolution of 13 m
- Determined the total peat carbon stock and its spatial variation in a large peatland area

Supporting Information:
Supporting Information may be found in the online version of this article.

Correspondence to:
P. Gao,
pegao@syr.edu

Citation:
Gao, P., Li, Z., Majumdar, A., & Li, Z. (2025). Determining spatially variable peat depths of an alpine peatland in the Qinghai-Tibet Plateau. *Journal of Geophysical Research: Biogeosciences*, *130*, e2024JG008713. https://doi.org/10.1029/2024JG008713

Received 5 JAN 2025
Accepted 16 MAY 2025

Author Contributions:
Conceptualization: Peng Gao
Data curation: Anwesha Majumdar
Formal analysis: Peng Gao, Zhuohong Li
Funding acquisition: Zhiwei Li
Investigation: Peng Gao
Methodology: Peng Gao, Zhuohong Li
Project administration: Zhiwei Li
Resources: Peng Gao
Software: Zhuohong Li
Supervision: Peng Gao
Validation: Peng Gao, Zhuohong Li
Visualization: Peng Gao
Writing – original draft: Peng Gao
Writing – review & editing: Peng Gao

Determining Spatially Variable Peat Depths of an Alpine Peatland in the Qinghai-Tibet Plateau

Peng Gao[1], Zhuohong Li[2], Anwesha Majumdar[1], and Zhiwei Li[3]

[1]Department of Geography and the Environment, Syracuse University, Syracuse, NY, USA, [2]State Key Laboratory of Information Engineering in Surveying, Mapping and Remote Sensing, Wuhan University, Wuhan, China, [3]State Key Laboratory of Water Resources Engineering and Management, Wuhan University, Wuhan, China

Abstract Understanding peat depths is crucial for assessing carbon dynamics within peatlands. However, accurately estimating peat depths across large areas remains challenging. In this study, we developed a novel approach integrating a machine-learning based regression modeling with an optimized field sampling strategy to predict spatially variable peat depths across the Black River (BR) watershed with an area exceeding 4,600 km^2 within the Zoige basin of the Qinghai-Tibet Plateau. Using the key controlling factors (elevation, slope, soil organic carbon, and soil bulk density), we created a high resolution (13 m) digital map depicting the spatial distribution of peat depths throughout the BR watershed. We validated the accuracy of predicted peat depths through comparison with field measurements and revealed that slope is the dominant control in determining peat depths. The resulting map highlights that deep peat deposits typically cluster in upslope sections and areas of higher elevations. The total peat carbon stock within the study area amounts to approximately 4.195 Pg C, following a spatial pattern similar to peat depths but with greater concentration in three specific counties. These high-resolution peat depth and peat carbon maps provide valuable insights for effective peatland management in these vulnerable alpine ecosystems.

Plain Language Summary In this study, we developed an innovative methodology for mapping peat depths across a vast 4,600 km^2 peatland landscape. By integrating optimized field sampling with machine learning regression models, we produced the first high-resolution (13 m) peat depth map of this scale with high accuracy. Our analysis revealed that elevation, slope, soil organic carbon, and soil bulk density are the primary determinants of peat depth, with slope emerging as the most influential factor. This detailed mapping enabled precise identification of spatial peat depth patterns and significantly improved carbon stock calculations compared to previous estimates based on simplified average depths.

1. Introduction

Peatlands represent specialized wetland ecosystems that function as Earth's predominant carbon reservoirs while simultaneously constituting major sources of global methane emissions (Gorham, 1991; Turetsky et al., 2014; Vepraskas & Craft, 2016; Yu et al., 2010), though they only take 3% of the global land area (Ballard et al., 2011; Holden, 2009). Climate change and intensified human activities have led to widespread peatland degradation across many regions of the world (Cole et al., 2022; Fenner & Freeman, 2011; Joosten & Clarke, 2002), resulting in elevated emissions of carbon and accelerated decreases of water storage in peatland-dominated ecosystems (Lou et al., 2014; Turetskey et al., 2014). Therefore, comprehensive knowledge of peatland volumes is fundamental for assessing the potential environment impacts of degraded peatlands. Significant research has been conducted to identifying peatland extents and areas at both local and global scales (Dargie et al., 2017; Donlan et al., 2016; IUCN, 2021; Melton et al., 2022; Rampi et al., 2014; Xu et al., 2018). However, data on spatially variable peat depths are essential for accurate calculation of peat volume, which is crucial for determining the total carbon and water storage losses resulting from peatland degradation (Strack et al., 2022; Temmink et al., 2023; Young et al., 2018). Furthermore, peat depths and their spatial variations function as critical controls influencing hydrological processes (Dixon et al., 2017) and serve as proxies for assessing biodiversity conservation capacity and optimized ecosystem service recovery (Crooks et al., 2011; Strack et al., 2022; Tan et al., 2022; Temmink et al., 2023).

Nonetheless, determining peat depths presents significant challenges, as field sampling is inevitably required regardless of whether the objective is modeling or mapping their spatial distribution (Minasny et al., 2019; Parry et al., 2012). In the field, peat depths can be manually probed using various soil coring devices (Charman, 2002;

Parry et al., 2012), leading to point samples of peat depths that can be further used to determine peat extent (Grant et al., 1997), date the time of peat formation (Chen et al., 2014), or examine peat properties (Dettmann et al., 2022; Householder et al., 2012; Wang et al., 2015). These direct methods are labor-intensive and are prone to disturbing peat health (Keaney et al., 2013; Li, Henrion, et al., 2024). Furthermore, they typically cover very limited areas of peatlands (e.g., 0.000032 km^2 in (Parry et al., 2012)). Alternative approaches involve indirect measurements, which use proximal sensors to gather geophysical signals (e.g., the apparent electrical conductivity or electromagnetic waves) that can be interpreted to infer peat depths (Beucher et al., 2020; Rosa et al., 2009; Slater & Reeve, 2002). While these methods avoid direct disturbance of peat soils, they still require physical transportation and movement of equipment across the survey area (Fyfe et al., 2014; Parsekian et al., 2012). Thus, the spatial extent of peatlands that can be practically surveyed using these methods remains relatively limited (e.g., around 0.01 km^2) (Beucher et al., 2020; Parsekian et al., 2012; Pezdir et al., 2021). This limit was overcome by using airborne Ground Penetrating Radar or Light Detection and Ranging to survey a larger area up to more than 400 km^2 (Boaga et al., 2020; Chasmer et al., 2017; Gatis et al., 2019; Keaney et al., 2013), but the estimated peat depths still need to be calibrated using the directly measured peat depth data (Keaney et al., 2013; Silvestri et al., 2019) or are in classes representing ranges of values (Lilja & Nevalainen, 2006).

A different type of approaches aim to predict continuous peat depths across varying spatial scales, commonly referred to as digital soil mapping techniques (Zhang et al., 2017), using diverse geostatistical modeling approaches (Akumu & McLaughlin, 2014; Gatis et al., 2019; Householder et al., 2012; Keaney et al., 2013; Parsekian et al., 2012; Plado et al., 2011). However, these models still require a subset of field-measured peat depth samples for calibration purposes. Recent advancements have led to the development of more sophisticated spatial models leveraging machine learning (ML) algorithms (Fadhurrahman & Saputro, 2022; Ivanovs et al., 2024; Li, Henrion, et al., 2024; Rudiyanto et al., 2018). Although these approaches produce more reliable peat depth maps compared to earlier methods, they continue to face two significant challenges. First, these approaches require field-collected peat depth measurement for proper model calibration and validation, which explains why their implementation has been widely confined to smaller areas where such depth samples have already existed. Second, while the predicted peat depths may cover extensive areas (spanning several hundred kilometers or more), they typically feature coarse spatial resolution (greater than 30 m) (Fadhurrahman & Saputro, 2022; Ivanovs et al., 2024). Employing Unmanned Aerial Vehicles to enhance the spatial resolution of terrain-related covariates can substantially improve the detail of predicted peat depth maps, but this method remains constrained to relatively smaller geographical areas (Li, Henrion, et al., 2024). Therefore, determining peat depths and their spatial distribution across vast peatland regions with both high resolution and accuracy continues to present significant challenges.

The Qinghai-Tibet Plateau houses the largest alpine peatland system in the world (Gaffney et al., 2024). This fragile ecosystem faces significant degradation due to climate change and intensified human activities, threatening its ecological integrity (Hou et al., 2020; Yang et al., 2017). These concerns have promoted numerous studies focused on carbon storage assessment (Chen et al., 2014; Lei et al., 2024; Luo et al., 2021; Wang et al., 2014; Zhang et al., 2023). However, existing assessment methods either depend on uniformly divided soil depths, potentially incorporating non-peat soils or missing some deeper peat layers, or utilize averaged peat depths derived from sparse field measurements. These methods fail to capture the spatial heterogenity of peat depths, thereby compromising accurate estimations of peatland volume and carbon storage capacity.

The purpose of this study is to develop a novel approach that combines a machine learning regression model with an optimized ground-sampling strategy to predict the spatial distribution of peat depths across a very large area (more than 4,000 km^2) in the remotely located Qinghai-Tibet Plateau at a finer resolution with high accuracy (Figure 1a). This approach allows us to examine the spatial characteristics of the predicted peat depths and calculate the total peat carbon stock (TPCS) with improved accuracy. Peatlands are areas where layers of partially decomposed organic material accumulate over underlying unconsolidated soil (IUSS, 2006; Moore, 1989). These layers should contain a minimum organic material content either 20% (Minasny et al., 2019) or 30% (Joosten & Clarke, 2002), depending on the classification system used. In this study, we define peat depth as the thickness of a layer containing partially decomposed organic matter exhibiting brown or dark colors (Christanis, 1994), measured from the surface to interface with the underlying mineral soils.

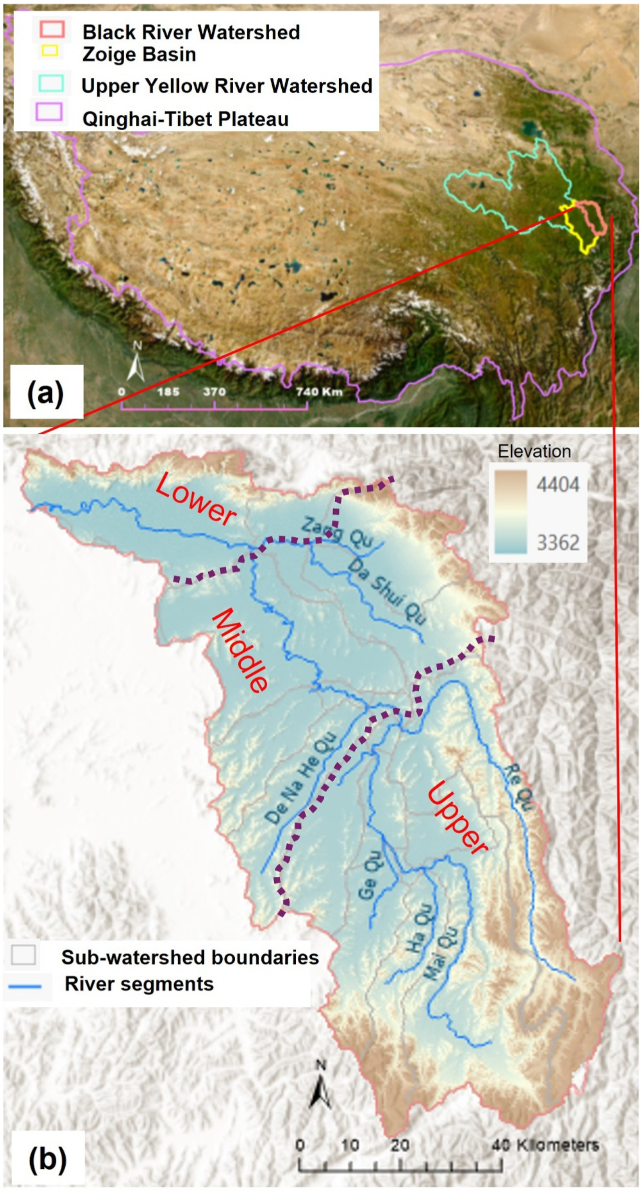

Figure 1. Geography and geomorphology of the study area. (a) The geographic location of the study area; (b) the geomorphological settings of the Black River watershed. The two dashed curves divide the Black River Watershed into three parts: the lower, middle, and upper parts.

2. Materials and Methods

2.1. Study Area

Our study focuses on the Black River (BR) watershed, a proportion of the Zoige basin that is a unique smooth upland area within the Upper Yellow River watershed, located on the northeastern side of the Qinghai-Tibet Plateau (Figure 1a). The BR watershed covers more than 4,600 km^2, taking about 47.5% of the total Zoige basin area (Li et al., 2015). It has a typical continental monsoon climate, characterized by long, dry winters and hot, wet summers. Its annual mean precipitation is 1,100–1,274 mm, while its annual mean temperature ranges between 0.6 and 1.2°C (Li et al., 2020). Being part of the Qinghai-Tibet Plateau, the BR watershed has high elevations varying from 3,362 to 4,404 m (Figure 1b) with an average of 3,518 m. Its topography demonstrates generally flat lands with gentle, relatively uniform slopes extending upslope through the watershed, which are dissected by discontinued rolling hills and low ridges on both sides of the watershed. According to this topographic characteristic, we divide the BR watershed into three parts, the lower, middle, and upper parts (separated by the two dashed curves in Figure 1b) for convenience of analysis. The relatively smooth topography was formed by relatively fast uplift of mountains surrounding the basin over millions of years (Li et al., 2011; Liu et al., 2021). The Black River is the main channel of the river system draining through the watershed from the south to the northwest. It is branched by seven main tributaries starting from the west and moving to the east in a count-clockwise order, De Na He Qu, Ge Qu, Ha Qu, Mai Qu, Re Qu, Da Shui Qu, and Zang Qu (Figure 1b). Based on these geomorphological characteristics, the BR watershed was divided into 19 sub-watersheds again for the purposes of analysis.

Sitting within the Zoige basin, which is known for its concentrated and extensive peatlands (Guo et al., 2013; Tan et al., 2022; Yang et al., 2017), the BR watershed is the core of a unique high-altitude ecosystem supporting water conservation and biodiversity (Joosten et al., 2008). Peatlands and grasslands are two main land cover types (Yu et al., 2017). Although peatlands are widely distributed over the entire BR watershed, they present in diverse forms, such as marshes, bogs, and fens, due to variations of local topography, hydrology, and nutrient inputs. As such, some studies concluded that these peatlands belong to the minerotrophic type (Gaffney et al., 2024; Ma et al., 2017), while others claimed that they pertain to the ombrotrophic one (Chen, et al., 2023). These apparent discrepancies suggest that peatland distribution is of strong spatial heterogeneity, because of spatially variable hydrological conditions, soil properties, and vegetation (Joosten & Schumann, 2007; Ma et al., 2017). Therefore, we expect that peat depths vary greatly across the BR watershed and their spatial pattern is complex.

3. Methods

As described previously, existing methods of assessing or measuring peat depths are inappropriate for determining the spatial distribution of peat depths in the BR watershed with a very large area (>4,600 km^2). For this reason, we developed a new approach that combines a machine learning regression model with an optimized peat-depth sampling strategy.

Peat Depth sampling. The remote location and limited local road network of the BR watershed indicate that it is impossible to manually collect ground-measured samples across the entire area. Alternatively, limited peat samples were taken in the summer of 2023 along the local roads and the sampling space ranged from 2 to 6 km to avoid local sampling clusters (i.e., inefficient sampling) and to cover as much area as possible (i.e., sufficient

Journal of Geophysical Research: Biogeosciences
10.1029/2024JG008713

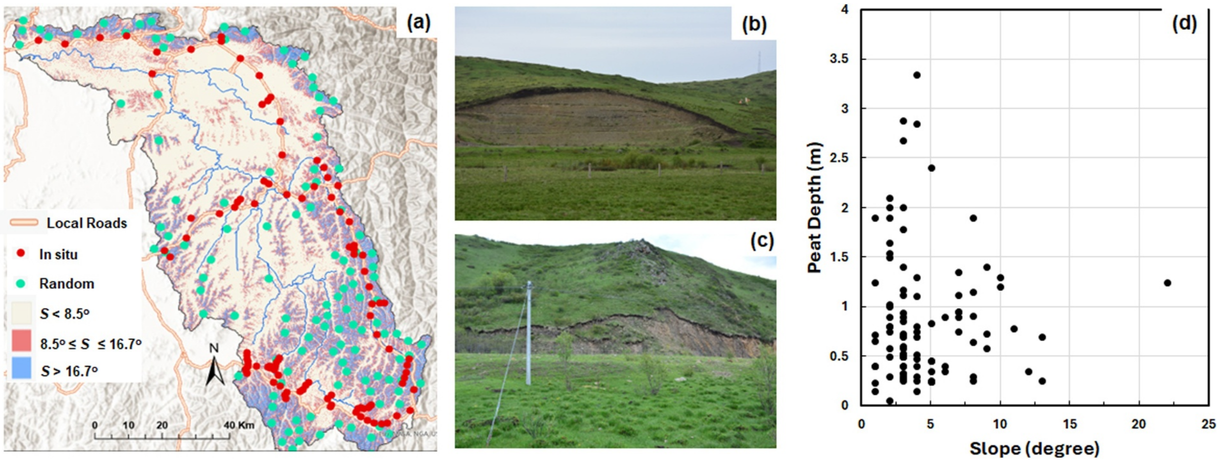

Figure 2. An optimized sampling schema for obtaining peat depths from the fields. (a) The two types of peat depth samples obtained across the study area. Red points were directly measured from the local sites, while green points were extracted from the areas with slope greater than 16.7°, which is represented by the small blue areas; (b, c) examples of the hills with the exposed bare soils that can be referred to for visually identifying the peat depths; (d) the relationship between the field-measured peat depths and the associated slopes of the ground.

sampling) (Figure 2a). The sampling sites were selected based on the micro-topographic features and ecological conditions of the peatland. For instance, locations with hummocks and ridges or grasslands underlain by distinct mineral soils were deliberately excluded from the sampling process. At each site, a soil auger of 0.08 m in diameter and 0.6 m in length was pushed downward to the ground. The bottom of the peat layer was judged by in situ examining structure, color, and component of the mixture of the organic matter and unconsolidated soil. In places with gullies and streams, we measured the peat depth from the vertical profile of the bank. Where the peat layer is thicker (>1.5 m), we used an automatic auger to drill a deep hole on the ground till the bottom of the peat layer was identified. Although point samples collected in this way roughly expand the entire watershed (Figure 2a), they show linear patterns that match the spatial distribution of local roads. Therefore, these samples are insufficient to represent peat depths in the spaces far away from the ground-measured samples. Unfortunately, these unsampled areas are physically difficult to access. However, we observed in our field campaigns that on local hills dividing these areas with steeper slopes, peat depths are all very shallow (Figures 2b and 2c), ranging between 0.05 and 0.3 m based on visual judgment and physical measurements (on some accessible hills). This observation is also consistent with peat depths on steep slopes of other regions (Li, Henrion, et al., 2024). By examining the relationship between peat depths and slopes of the ground-sampled sites (Figure 2d), we determined that the threshold slope above which peat depth is shallow is about 16.7°. This is the slope that typically breaks the steep hills from the gently declined smooth areas. We then extracted the areas with slope greater than 16.7° and randomly selected the number of points similar to those directly measured and assigned a peat depth within this range (Figure 2a). Combining the two leads to the final field-obtained samples of peat depths with 224 points.

Peat depth determination. The spatially variable peat depths over the large study area were determined using a machine-learning based regression modeling analysis. The fundamental hypothesis bolstering this approach states that the spatially variable peat depths may be accurately estimated using known information of topography, soil properties, and ground-measured peat depth samples. The first step is data processing (Figure 3a). We managed to collect and compile four data sets reflecting topological and soil conditions of the study area that are related to peat depths. They are Elevations, Slopes, Soil Organic Carbon (SOC), and Soil Bulk Density (SBD):

- Elevations. The Digital Elevation Model (DEM) data was downloaded from the site containing the data obtained from the Advanced Land Observing Satellite: https://search.asf.alaska.edu/#/?dataset=ALOS. This DEM has a spatial resolution of 12.5 m. The downloaded DEM was subsequently mosaiced and clipped to the BR watershed in ArcGIS Pro 3.3.1.
- Slopes. Using the compiled ALSO DEM data, slopes with the same spatial resolution were calculated using ArcGIS Pro 3.3.1 in degree for the entire study area.

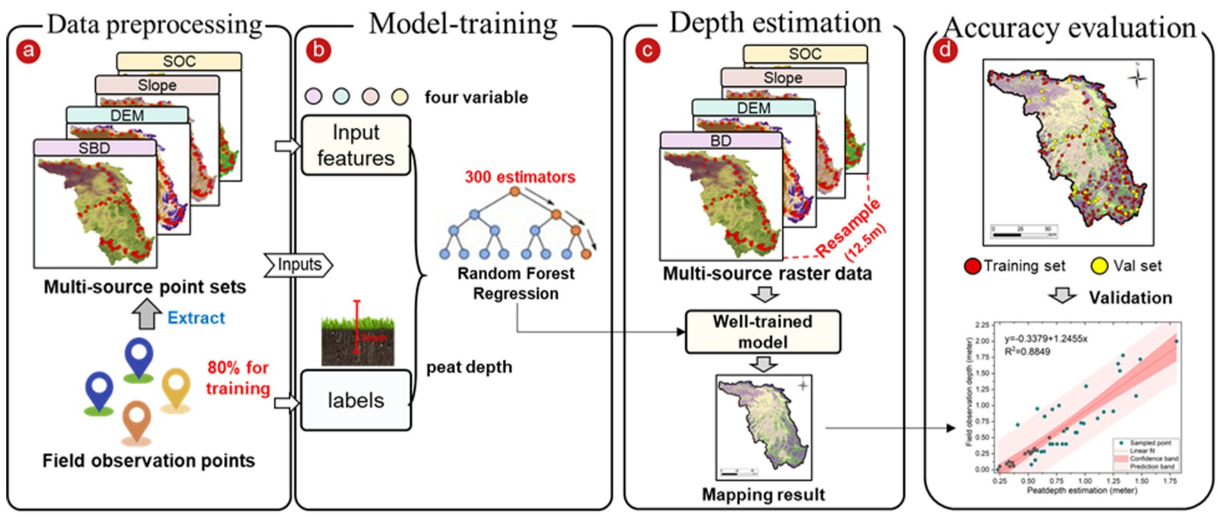

Figure 3. The procedure of the proposed machine learning based regression model.

- SOC. This data was generated from recently developed high resolution National Soil Information Grids of China with the resolution of 90 m (Liu et al., 2022). The data were generated using a state-of-the-art ensemble machine learning method coupled with high-resolution soil-forming environment characterization. They involve SOC values in each of the six soil layers from the ground downward: 0–0.05, 0.05–0.15, 0.15–0.30, 0.30–0.60, 0.60–1.00, and 1.00–2.00 m. We created a comprehensive SOC layer by linearly combining the SOC values in the six layers with variable weights, higher in top layers, while lower in lower layers.
- SBD. This data was created based on the original SBD values of six layers from the same source (Liu et al., 2022). Using a similar liner model to that for SOC, we generated a single layer representing the combined SBD values across the study area.

Elevation and slope are geomorphological structures that implicate the physical settings under which peats were formed. SOC reflects the content of humus, animal and plant residues, and microorganisms formed by microbial interactions in soil, while SBD reflects the ratio of soil mass after drying to the mass before drying for a certain volume. Both SOC and SBD are clearly related to peat depths. These four data sets were subsequently used as inputs for depth estimation.

The second step is training a Machine Learning (ML) regression model in terms of the field-obtained samples (Figure 3b). We utilized a random forest regression model (Breiman, 2001) with 300 estimators for determining the peat depths in the study area. To train this model, we sampled four input data sets (i.e., DEM, Slope, SOC, and SBD) according to the locations of the 224 field-observed and randomly selected points. These peat depth samples serve as labels to link the known peat depth values to the combined values of the four variables. We randomly selected 80% of the sampling points as the training data set, which ended up with 178 sample points (Figure 3b). The selected points with field-observed peat depth labels are grouped into 4 × 178 values (variables × sampling points) to feed the random forest regression model for training. Finally, all parameters of the model used to estimate peat depth were determined during the training process. In the third step (Figure 3c), the well-trained regression model was used to estimate peat depths of the entire study area based on the above-mentioned four input data sets. In this process, the model sequentially scans each of the four raster data sets to capture the four variables as the model inputs and predicts the peat depth at each location of the study area. After predicting the entire study area using the trained ML model, we post-processed the predicted peat depth values by stretching the maximum and minimum values in the predicted peat depth map, such that they match the range of the field-observed values in the study area. The fourth step (Figure 3d) is to estimate the accuracy of the predicted peat depths. For this purpose, we retained 20% (46 points) of the field-obtained sample points as the validation data, which were selected to assure that they extend over the entire study area as much as possible (Figure 3d). For accuracy estimation, we calculated commonly used metrics, such as mean square error (MSE), mean absolute error (MAE), and coefficient of determination (R^2), to comprehensively evaluate the prediction results of the region. We also conducted parameter setting optimization and sensitivity analyses for the four input variables.

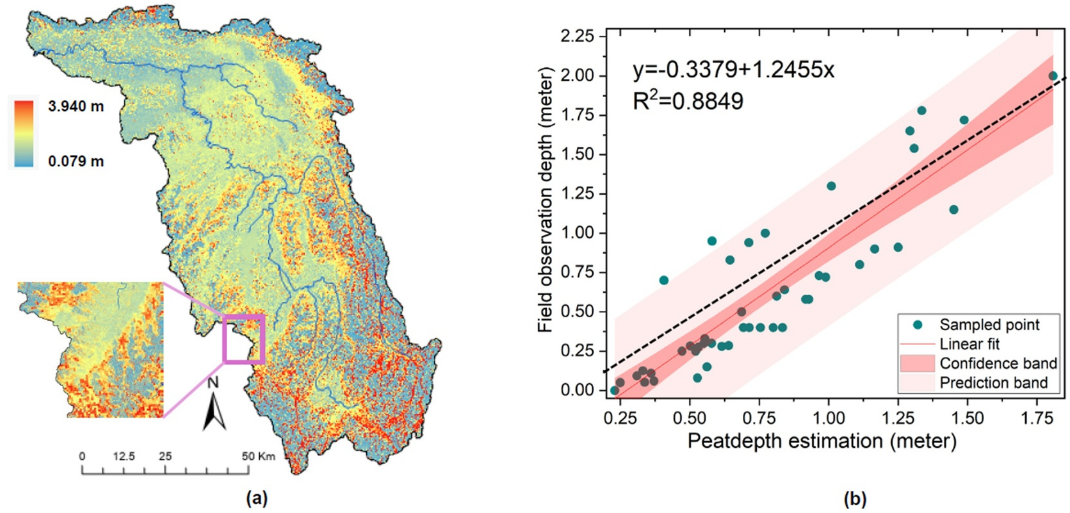

Figure 4. The results from the machine learning based regression model. (a) The predicted peat depths over the study area (the Black River Watershed). The inset shows an enlarged peat depths within a small portion; (b) an example of accuracy assessment (R^2).

4. Results

4.1. Peat Depths and Their Spatial Distribution

Our machine learning based modeling analysis produced a digital map showing the spatially variable peat depths within the Black River watershed at the spatial resolution of 13 m (Figure 4a). The accuracy assessment gave rise to MSE = 0.0865 m, MAE = 0.2851 m^2, and R^2 = 0.8849. In the case of R^2, the majority of the 46 points were plotted within or near the confidence interval and almost all of the points were within the prediction band (Figure 4b). These results indicate that the predicted peat depth distribution is robust and accurate at this fine spatial resolution (13 m). Our sensitivity analysis identified Slope as the most important variable for determining peat depths, with its importance substantially exceeding the other three variables (Figure S1 in Supporting Information S1). While DEM showed a slightly greater importance than SOC and SBD, the difference was modest. These findings indicate that topographical factors primarily control peat depth distribution, though the contributions of SOC and SBD remain relevant considerations.

The spatial distribution of peat depths demonstrates a striking nature of the geospatial pattern: peatlands with deep depths (>0.8 m, reddish color in Figure 4a) are well blended with shallow peatlands (0.3–0.8 m, yellowish color in Figure 4a), which are further divided by shallow peatlands on hills (<0.3 m, blueish color in Figure 4a). The implication is that in an apparently continuous large peatland area as typically shown in peat maps, peats do not have similar soil properties because their depths vary greatly. Therefore, this peat depth map provides much richer and accurate information about the biological status of peats than the widely available peat maps only showing the extents of peats.

4.2. The Geospatial Patterns of the Peat Depths

Many organizations, including the World Reference Base for soil resources (FAO, 2022), the US Department of Agriculture (Kolka et al., 2011), and the National Wetlands Working Group (NWWG, 1997), classify peatland as an unconsolidated soil layer comprising organic materials that extend to a minimum depth of 0.4 m. Other institutions and researchers have employed a 0.3 m threshold depth (UNEP, 2022; Wittnebel et al., 2021). In our study area (i.e., the Black River watershed), comparison of the vertical SOC profiles at ground-measuring locations with peat depths between 0.25–0.3 m and 0.4–0.5 m (Figure 5) reveals similar soil organic properties in these layers, aligning with our multi-year field observation. Given these varying definitions of peat soils, we adopted a compromise approach for selection, defining healthy peatlands as the areas whose peat depth is equal or greater than 0.3 m, treating lands with peat depths between 0.15 and 0.3 m as degraded peatlands, and classifying areas with peat depth below 0.15 m as non-peat. Based on this classification, we produced a fine-resolution (13 m)

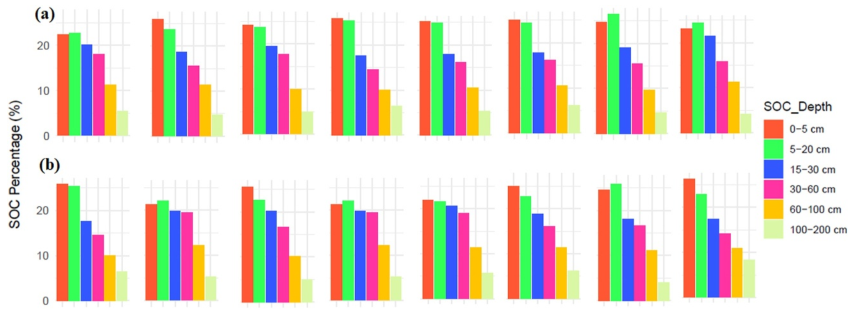

Figure 5. Percentage of Soil Organic Carbon in the six consecutive vertical layers for samples with peat depths of (a) 0.25–0.3 m and (b) 0.4–0.5 m.

peat classification map (Figure 6a). In the upper-reach areas (i.e., the upper part in Figure 1), peatlands in the upstream half section are densely dissected by degraded peatlands of smaller clusters, while in the middle part, they tend to be more continuously extended over the middle area with gentle slopes, but still segregated by degraded peatlands on both edges with steeper slopes. In the lower part, healthy peatlands are widely fragmented by degraded peatlands (Figure 6a). Overall, about 78% of the entire Black River watershed is covered by healthy peatlands. This percentage seems higher than what reported in earlier studies (Chen et al., 2014), possibly because of (a) different study areas, and (b) different definitions of healthy peatlands.

Within the healthy peatlands, peat depth still varies from 0.3 to possibly more than 4 m. Therefore, their hydrological and ecological significance, as well as potential impact on climate change would be drastically different in different locations. To reveal this spatial variation, we identified clusters of deep peatlands by performing hot spot analysis, which is a type of geostatistical technique. The deep peatland is defined here as the area whose peat depth is >0.8 m. This threshold is selected based on the spatial distribution of peat depths in the entire Black River watershed. The clusters of deep peats are mainly distributed in the upper and middle parts of the Black River Watershed (Figure 6b). They present in elongate shapes primarily following the orientations of the local river channels, but most of them are not located in river valleys.

To better characterize the complexity of the spatial patterns of the deep peatlands, we examined the area percent of the deep peatlands (%A) in each of the 19 sub-watersheds covering the Black River watershed. Along each of the seven main tributaries to the Black River (Figure 1), %A is high in the upper contributing area and decreases significantly moving down to the lower lands of the same watershed (Figure 7a). This trend is consistent in all sub-watersheds following the seven major tributaries. It indicates that deep peatlands generally are located in

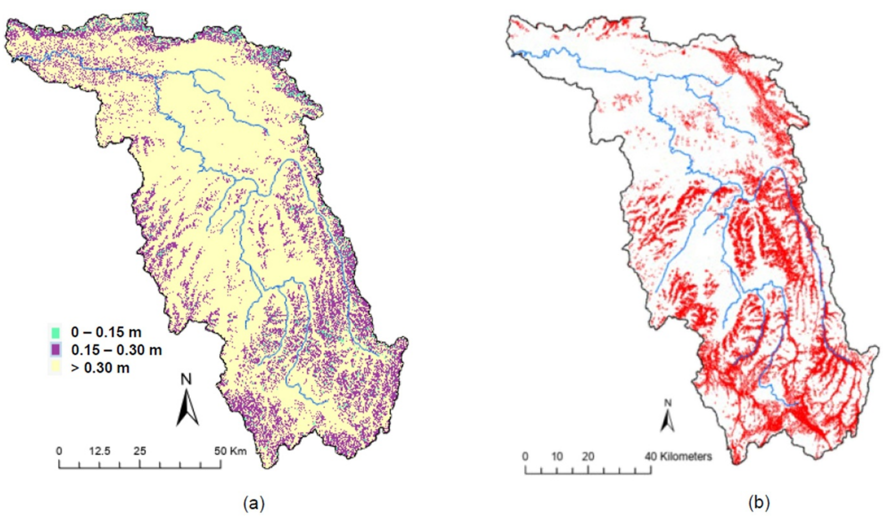

Figure 6. (a) Peatland classification based on depth variations: light green – no peats, purple – degraded peats, yellow – healthy peats; (b) spatially clustered deep peats (red color).

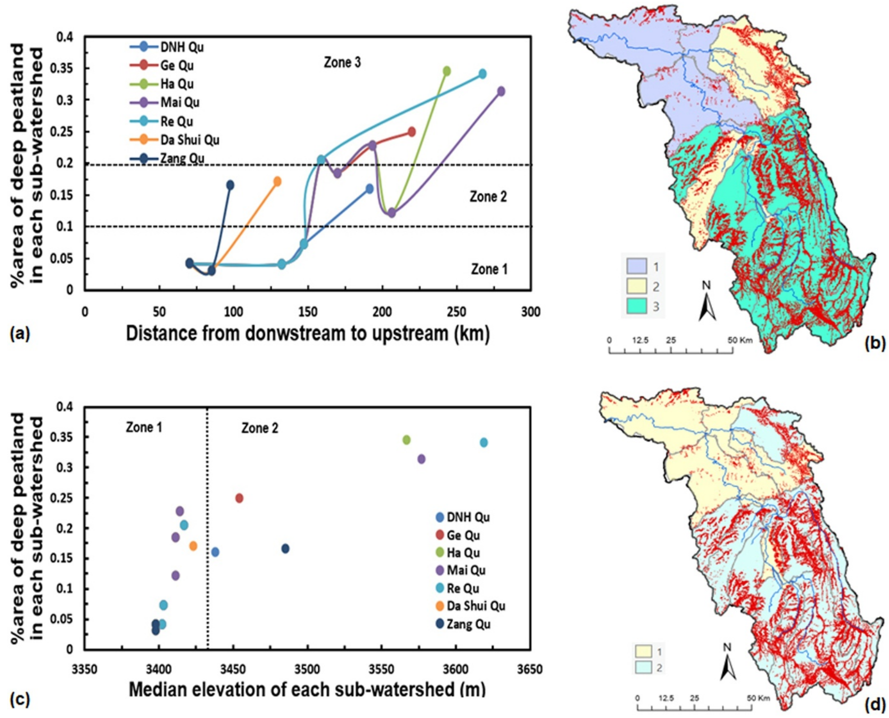

Figure 7. Geospatial patterns of clustered deep peatlands. (a) Longitudinal changes of %A in sub-watersheds along each of the seven main tributaries of the study area; (b) the spatial distribution of the three zones with distinct values of deep peats; (c) Changes of %A with regard to the median elevations of sub-watersheds; (d) the spatial distribution of deep peats based on elevations.

geomorphological upstream portions of all sub-watersheds and can be divided into three zones (Figures 7a and 7b). Zone 1 has less than 10% of deep peatlands, most of which have less than 5%. They are located in the lower middle parts of the Black River watershed. Zone 2 holds the deep peatlands between 10% and 20% and is typically distributed in the northeast of the lower part and some areas of the middle part of the Black River watershed (Figure 7b). Zone 3 contains deep peatlands above 20% and could be up to 35%. They dominate the middle and upper parts of the Black River watershed.

The spatial patterns of the deep peatlands can also be characterized in terms of elevation. Along each of the seven main tributaries, %A increases as elevation (represented as the median of elevations in each sub-watershed) increases (Figure 7c). There is a clear break point of the slopes in the general %A-elevation trend around the median elevation of 3,425 m. Based on this pattern, the Black River watershed may be divided into two zones (Figure 7d). Zone 1 in the lower and middle parts of the Black River watershed, in which %A increases faster with elevation, though the absolute values of %A are generally small. Zone 2 mostly in the middle and upper parts of the Black River watershed where %A increases gently with elevation, but the values of %A are generally high (Figure 7d). These results indicate that at broader spatial scales (i.e., sub-watersheds), topographic elements including elevations and slopes exert primary control over the spatial variability of peat depths, an inference that is consistent with existing research (Sun et al., 2023).

5. Discussion

5.1. Peat Depths at Different Spatial Resolution

In this study, we produced a digital map of peat depths over an area of more than 4,600 km^2 (i.e., the Black River (BR) watershed) with the spatial resolution of 13 m. This is by far the finest spatial scale at which peat depths are determined over a very large area. Thus, it has a great potential for being used to accurately determine the effects of peatlands on hydrology and ecosystems under the influence of climate change. In this map, each point of the value reflects an aggregated value of peat depths over an area of 13 × 13 m. This value is different from a peat depth obtained in the field at a point location. To illustrate this discrepancy, we compared the peat depths

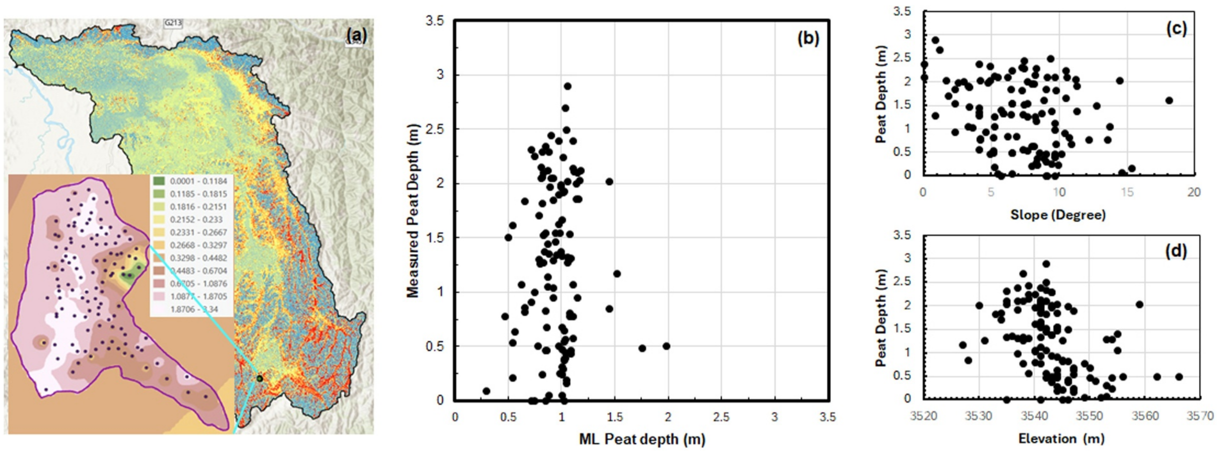

Figure 8. The differences of peat depths at two different spatial scales. (a) Peat depths in the Black River Watershed and a very small watershed of 0.1 km^2 within it. The continuous distribution of peat depths within the small watershed was generated using an interpolation method (inverse distance weighted); (b) comparison of peat depths obtained at two different spatial scales; (c) the relationship between peat depths and elevations in the very small watershed; (d) the relationship between peat depths and slopes in the very small watershed.

determined using our machine learning modeling method with those directly measured in a very small watershed of 0.1 km^2. Compared with the entire BR watershed, this area appears as a point when it is scaled to the BR watershed (Figure 8a). In one of our earlier studies (Li & Gao, 2020), we manually measured peat depths at 119 locations within this very small area (Figure 8a). The subsequent spatial interpolation analysis based on the inverse distance weighted method showed that peat depth varies greatly even across this small area, ranging from almost zero to about 3 m. However, when peat depths at these locations were extracted from the map produced in this study, they range between 0.28 and 2 m with most values centering on 1 m (Figure 8b). Comparison of the two data sets (Figure 8b) signifies that the machine learning modeling method used in this study smooths out variations of peat depths at finer spatial scales, suggesting that peat depths are more dynamic at finer spatial scales (Gallant et al., 2018). It also suggests that the predicted peat depths at this spatial scale (i.e., 13 × 13 m) smooth out the actual variations of peat depths within this scale, similar to the results from other methods (Parsekian et al., 2012). This upscaling effect means that our peat depth map is valuable for accurate estimation of C stock in this area and large-scale peatland management, but it should not be used for distinguishing differences of peat depths in individual locations.

It is also interesting to notice that even within the very small area of 0.1 km^2, peat depths are not correlated with either elevations or slopes (Figures 8c and 8d). The implication is that at least in the study area (i.e., the BR watershed), peat distribution is not directly controlled by geomorphological structure. This might be related to the historical development of peatlands. In the Zoige basin that includes the study area, the lands have experienced complicated tectonic movements, which lasted over tens of thousands of years. As such, peats in this region actually were developed in different geological times, each of which may have different topographic structures (Gaffney et al., 2024; Wang, M et al., 2015). Therefore, developing topography-based models for predicting peat depths (Parry et al., 2012) is not reliable for our study area. We believe that the newly developed machine learning based model is the best for determining peat depths over a very large area.

5.2. Total Peat Carbon Stock and Its Spatial Distribution

Since we have already known spatially variable SOC and SBD along vertical profiles down to 2 m below the ground, the developed map of peat depths allows us to empirically calculate the total organic carbon in peatlands of the study area:

$$C_t = \sum_{i=1}^{n} C_i \times BD_i \times D_i \tag{1}$$

where C_t is total organic carbon in peat (Pg C, 1 Pg = 10^{15} g), C_i is the SOC in the area of a single grid cell (13 × 13 m), BD_i is the associated SBD in peat, D_i is the mean peat depth within each cell, and n is the total

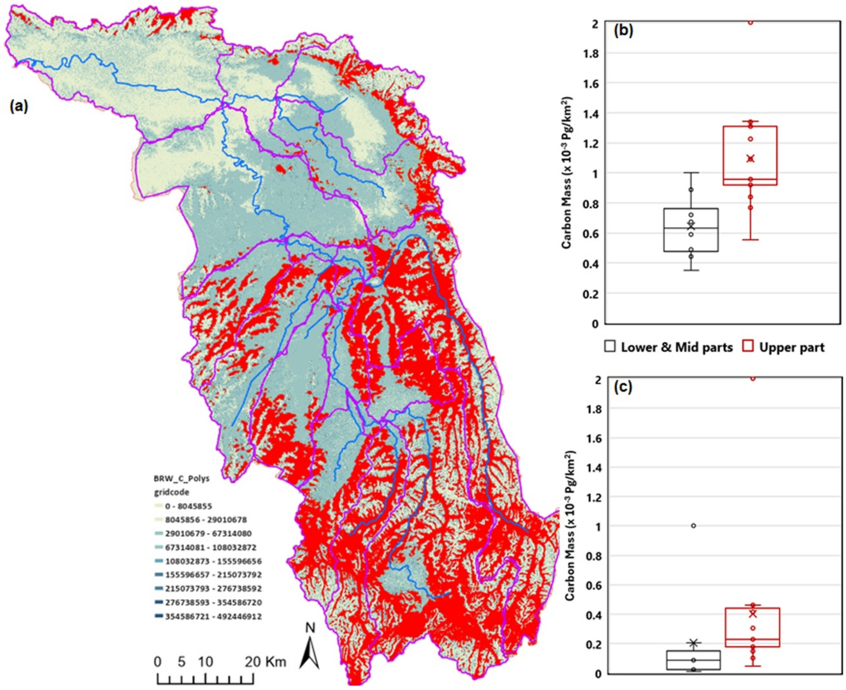

Figure 9. The total peat carbon stock (TPCS) and its spatial patterns. (a) Spatial distributions of TPCS. The red color represents the local clusters of high TPCS (i.e., hot spots); (b) statistical differences of TPCS between upper and middle and lower parts of the Black River watershed; (c) statistical differences of high-value clusters of TPCS between the two parts.

number of grid cells covering the entire study area. This calculation considers the spatial variations of peat soil properties and should be more accurate than the previous methods (Chen et al., 2014; Law et al., 2015; Minasny et al., 2019). The TPCS in the BR Watershed is about 4.195 Pg C. This value is higher than those in previous studies (Wang et al., 2014; Yang et al., 2017; Zhang et al., 2023), but within the same order of magnitude. It is important to note that this comparison has limitations, as the carbon calculation methods vary across studies and peat volumes differ due to the use of different peat depth values. The spatial pattern of carbon distribution may represent the more significant finding from our analysis. Spatially, the peat carbon stock varies greatly across the BR watershed (Figure 9a). However, it is generally higher in the upper part of the BR watershed with the mean of 1.018×10^{-3} Pg/km^2 than that in the lower and middle parts (5.948×10^{-4} Pg/km^2) (Figure 9b). This spatial heterogeneity is more evident when hot spots, which refer to the statistically significant local clusters of high values of peat carbon stock, were identified using geostatistical analysis (Figures 9a and 9c). The mean of high-value clusters in the upper part (i.e., 2.66×10^{-4} Pg/km^2) is more than three times higher than that for the lower and middle parts (i.e., 7.51×10^{-5} Pg/km^2). Clearly, peatland conservation management should focus on the upper part of the BR watershed. Specifically, the conservation plans should be applied with high priority to Maiwa, Sedi, and Banyou counties, which cover most areas of the upper part.

5.3. Implication of Our Approach

The success of our approach for predicting large-area (>4,600 km^2) and high-resolution (13 m) peat depths with high accuracy mainly relies on two factors: (a) availability of some independent variables with a high-resolution (12.5 m) in the ML-based regression model and (b) development of an optimized, ground-based sampling strategy. The 12.5-m elevation and slope input data provide some high-resolution information across the entire, large study area that facilitates accurate predictive results, though other input variables (SOC and SBD) are only available at coarser resolutions. The optimized sampling method generated a set of point values of peat depths covering the whole study area, which allow for accurate model calibration and validation. Combination of these two factors guaranties that our new regression model is parsimonious and efficient. Although deep-learning based Convolutional Neural Network methods may produce land cover maps with the spatial resolution as fine as 1 m (Li, He, et al., 2024), they need training samples (i.e., labels) in the form of polygons or image patches. Obtaining such a set of samples means to measure substantially more peat depths, which are impossible in the study area that is located in remote regions and hard to access physically.

The spatial resolution of 13 m in our predicted peat depth map is determined by the resolutions of some input variables (i.e., elevations and Slopes). If there were even higher resolution (e.g., 6 m) DEM available, could we produce a digital map of peat depths at the spatial resolution of 6 m? The answer is no, because predicting peat depths at this finer scale would require substantially more training samples than our analysis used, in order to account for spatial variations in peat depths, bulk density, and soil carbon content - data that is practically impossible to obtain due to logistical constraints. Furthermore, the predicted peat depth in a given grid cell of certain resolution is the average of all variable peat depths within the cell (Figure 8b). Therefore, the resolution of a predicted peat depth map is essentially a trade-off between the spatial resolution of some input variables and the number of possibly obtained training samples. In other words, when our approach is applied to other peatland areas, a spatial resolution of <30 m is sufficiently high for a peat depth map over large areas compared with the existing peat depth maps with much coarser resolutions. It should be noted that in areas where SOC and SBD are not available, multi-spectral indices, such as Normalized Difference Vegetation Index, and Normalized Difference Water Index may be used as input variables for model prediction.

6. Conclusions

Determining spatially variable peat depths over a very large area is still a challenging task nowadays. In this study, we developed a new approach that has successfully predicted highly variable peat depths in the Black River watershed with an area of more than 4,600 km^2, which is a portion of the Zoige basin in the Qinghai-Tibet Plateau. This approach combines a machine-learning based regression model with an optimized sampling strategy for measuring peat depths. It is parsimonious and can be applied in other peatland regions of the world. In this study, the new approach allowed us to produce a digital map of peat depths for the entire Black River watershed with the spatial resolution of 13 m. The map shows that in the apparently continuous peatlands within the Black River watershed, peat depths are featured by high degrees of mixture among low, middle, and deep peats, implying the spatially variable peat properties and the associated carbon stock. Deeper peats are mainly concentrated in the upper part of the watershed and typically distributed in elongate shapes following the orientations of local rivers, but not in their immediate valleys. They also tend to lie in higher elevation areas. In the Black River watershed, the TPCS is about 4.195 Pg C, higher, but in the same order of magnitude as those in previous studies. Not only do the developed high-resolution peat depth and the associated carbon stock maps facilitate examining carbon dynamics of peat and developing best peatland management practices, but also the developed new method of predicting peat depth may be extended to other large peatlands in remote alpine regions.

Data Availability Statement

The digital map of peat depths created in this study is available here: Gao, P. (2025). Peat Depth Distribution in the Black River Watershed. Zenodo. https://doi.org/10.5281/zenodo.14601807.

Acknowledgments
We thank the two anonymous reviewers whose comments and suggestions help to improve the quality of the paper. This study is partly supported by the National Natural Science Foundation of China (U2243214 and 52479073).

References

Akumu, C. E., & McLaughlin, J. W. (2014). Modeling peatland carbon stock in a delineated portion of the Nayshkootayaow river watershed in Far North, Ontario using an integrated GIS and remote sensing approach. *Catena (Cremlingen)*, *121*, 297–306. https://doi.org/10.1016/j.catena.2014.05.025

Ballard, C. E., McIntyre, N., Wheater, H. S., Holden, J., & Wallage, Z. E. (2011). Hydrological modelling of drained blanket peatland. *Journal of Hydrology*, *407*(1–4), 81–93. https://doi.org/10.1016/j.jhydrol.2011.07.005

Beucher, A., Koganti, T., Iversen, B. V., & Greve, M. H. (2020). Mapping of peat thickness using a multi-receiver electromagnetic induction instrument. *Remote Sensing*, *12*(15), 2458. https://doi.org/10.3390/rs12152458

Boaga, J., Viezzoli, A., Cassiani, G., Deidda, G. P., Tosi, L., & Silvestri, S. (2020). Resolving the thickness of peat deposits with contact-less electromagnetic methods: A case study in the Venice coastland. *Science of the Total Environment*, *737*, 139361. https://doi.org/10.1016/j.scitotenv.2020.139361

Breiman, L. (2001). Random forests. *Machine Learning*, *45*(1), 5–32. https://doi.org/10.1023/a:1010933404324

Charman, D. J. (2002). *Peatlands and environmental change* (p. 320). John Wiley & Sons.

Chasmer, L. E., Hopkinson, C. D., Petrone, R. M., & Sitar, M. (2017). Using multitemporal and multispectral airborne lidar to assess depth of peat loss and correspondence with a new active normalized burn ratio for wildfires. *Geophysical Research Letters*, *44*(23), 11851–11859. https://doi.org/10.1002/2017gl075488

Chen, H., Yang, G., Peng, C., Zhang, Y., Zhu, D., Zhu, Q., et al. (2014). The carbon stock of alpine peatlands on the Qinghai–Tibetan Plateau during the Holocene and their future fate. *Quaternary Science Reviews*, *95*, 151–158. https://doi.org/10.1016/j.quascirev.2014.05.003

Chen, X. H., Xue, D., Wang, Y., Qiu, Q., Wu, L., Wang, M., et al. (2023). Variations in the archaeal community and associated methanogenesis in peat profiles of three typical peatland types in China. *Environmental Microbiome*, *18*(1), 48. https://doi.org/10.1186/s40793-023-00503-y

Christanis, K. (1994). The genesis of the NISSI peatland (northwestern Greece) as an example of peat and lignite deposit formation in Greece. *International Journal of Coal Geology*, *26*(1–2), 63–77. https://doi.org/10.1016/0166-5162(94)90032-9

Cole, L. E. S., Åkesson, C. M., Hapsari, K. A., Hawthorne, D., Roucoux, K. H., Girkin, N. T., et al. (2022). Tropical peatlands in the anthropocene: Lessons from the past. *Anthropocene*, *37*, 100324. https://doi.org/10.1016/j.ancene.2022.100324

Crooks, S., Herr, D., Tamelander, J., Laffoley, D., & Vandever, J. (2011). Mitigating climate change through restoration and management of coastal wetlands and near-shore marine ecosystems: Challenges and opportunities.

Dargie, G. C., Lewis, S. L., Lawson, I. T., Mitchard, E. T. A., Page, S. E., Bocko, Y. E., & Ifo, S. A. (2017). Age, extent and carbon storage of the central Congo Basin peatland complex. *Nature*, *542*(7639), 86. https://doi.org/10.1038/nature21048

Dettmann, U., Frank, S., Wittnebel, M., Piayda, A., & Tiemeyer, B. (2022). How to take volume-based peat samples down to mineral soil? *Geoderma (Amsterdam)*, *427*, 116132. https://doi.org/10.1016/j.geoderma.2022.116132

Dixon, S. J., Kettridge, N., Moore, P. A., Devito, K. J., Tilak, A. S., Petrone, R. M., et al. (2017). Peat depth as a control on moss water availability under evaporative stress. *Hydrological Processes*, *31*(23), 4107–4121. https://doi.org/10.1002/hyp.11307

Donlan, J., O'Dwyer, J., & Byrne, K. A. (2016). Area estimations of cultivated organic soils in Ireland: Reducing GHG reporting uncertainties. *Mires & Peat*, *18*.

Fadhurrahman, M., & Saputro, A. H. (2022). Peat depth prediction system using long-term MODIS data and random forest algorithm: A case study in Pulang Pisau, Kalimantan. Paper presented at 2022 1st International Conference on Information System & Information Technology (ICISIT). 2022 1st International Conference on Information System & Information Technology (ICISIT). (pp. 364–369). https://doi.org/10.1109/icisit54091.2022.9872550

FAO. (2022). World Reference Base for Soil Resources: International soil classification system for naming soils and creating legends for soil maps (Update 2022 of the 4th edition). *Food and Agriculture Organization of the United Nations*. Retrieved from https://openknowledge.fao.org/handle/20.500.14283/bcdecec7-f45f-4dc5-beb1-97022d29fab4

Fenner, N., & Freeman, C. (2011). Drought-induced carbon loss in peatlands. *Nature Geoscience*, *4*(12), 895–900. https://doi.org/10.1038/ngeo1323

Fyfe, R. M., Coombe, R., Davies, H., & Parry, L. (2014). The importance of sub-peat carbon storage as shown by data from Dartmoor, UK. *Soil Use & Management*, *30*(1), 23–31. https://doi.org/10.1111/sum.12091

Gaffney, P. P. J., Tang, Q. H., Li, Q. W., Zhang, R. Y., Pan, J. X., Xu, X. M., et al. (2024). The impacts of land-use and climate change on the Zoige peatland carbon cycle: A review. *Wiley Interdisciplinary Reviews-Climate Change*, *15*(1). https://doi.org/10.1002/wcc.862

Gallant, A. L., Sadinski, W., Brown, J. F., Senay, G. B., & Roth, M. F. (2018). Challenges in complementing data from ground-based sensors with satellite-derived products to measure ecological changes in relation to climate-lessons from temperate wetland-upland landscapes. *Sensors-Basel*, *18*(3), 880. https://doi.org/10.3390/s18030880

Gatis, N., Luscombe, D. J., Carless, D., Parry, L. E., Fyfe, R. M., Harrod, T. R., et al. (2019). Mapping upland peat depth using airborne radiometric and lidar survey data. *Geoderma (Amsterdam)*, *335*, 78–87. https://doi.org/10.1016/j.geoderma.2018.07.041

Gorham, E. (1991). Northern peatlands - Role in the carbon-cycle and probable responses to climatic warming. *Ecological Applications*, *1*(2), 182–195. https://doi.org/10.2307/1941811

Grant, M., Tomlinson, R. W., Harvey, J., & Murdy, C. (1997). Report from peatland survey end profiling project 1996/97. Environment and Heritage Service Research and Development Series. No. RC97.

Guo, C. X., Luo, F., Ding, X., Luo, Q., Luo, C. X., Cai, Y., et al. (2013). Palaeoclimate reconstruction based on pollen records from the Tangke and Riganqiao peat sections in the Zoige Plateau, China. *Quaternary International*, *286*, 19–28. https://doi.org/10.1016/j.quaint.2012.09.027

Holden, J. (2009). Upland hydrology. In A. Bonn, T. E. H. Allott, K. Hubacek, & J. Stewart (Eds.), *Drivers of change in upland environments* (pp. 113–134). Routledge.

Hou, M. J., Ge, J., Gao, J. L., Meng, B. P., Li, Y. C., Yin, J. P., et al. (2020). Ecological risk assessment and impact factor analysis of alpine wetland ecosystem based on LUCC and boosted regression tree on the Zoige plateau, China. *Remote Sensing*, *12*(3), 368. https://doi.org/10.3390/rs12030368

Householder, J. E., Janovec, J. P., Tobler, M. W., Page, S., & Lahteenoja, O. (2012). Peatlands of the Madre de Dios River of Peru: Distribution, Geomorphology, and Habitat Diversity. *Wetlands*, *32*(2), 359–368. https://doi.org/10.1007/s13157-012-0271-2

International Union of Soil Sciences (IUSS) Working Group. (2006). *World reference base for soil resources 2006: A framework for international classification, correlation and communication (world soil resources reports no. 103)*. Food and Agriculture Organization of the United Nations (FAO). Retrieved from https://www.fao.org/3/a0515e/a0515e00.pdf

IUCN. (2021). Peatlands and climate change. Retrieved from www.iucn.org/sites/default/files/2022-2004

Ivanovs, J., Haberl, A., & Melniks, R. (2024). Modeling geospatial distribution of peat layer thickness using machine learning and aerial laser scanning data. *Land*, *13*(4), 466. https://doi.org/10.3390/land13040466

Joosten, H., & Clarke, D. (2002). *Wise use of mires and peatlands*, International mire conservation group and international peat society.

Joosten, H., Haberl, A., & Schumann, M. (2008). Degradation and restoration of peatlands on the Tibet Plateau. *Peatlands International*, *1*, 31–35.

Joosten, H., & Schumann, M. (2007). Hydrogenetic aspects of peatland restoration in Tibet and Kalimantan. *Global Environmental Research*, *11*, 195–204.

Keaney, A., McKinley, J., Graham, C., Robinson, M., & Ruffell, A. (2013). Spatial statistics to estimate peat thickness using airborne radiometric data. *Spatial Statistics*, *5*, 3–24. https://doi.org/10.1016/j.spasta.2013.05.003

Kolka, R. K., Sebestyen, S. D., Verry, E. S., & Brooks, K. N. (Eds.). (2011). *Peatland biogeochemistry and watershed hydrology at the Marcell experimental forest*. CRC Press. Retrieved from https://www.fs.usda.gov/nrs/pubs/jrnl/2015/nrs_2015_kolka_001.pdf

Law, E. A., Bryan, B. A., Torabi, N., Bekessy, S. A., McAlpine, C. A., & Wilson, K. A. (2015). Measurement matters in managing landscape carbon. *Ecosystem Services*, *13*, 6–15. https://doi.org/10.1016/j.ecoser.2014.07.007

Lei, J. J., Zeng, C. L., Zhang, L., Wang, X. G., Ma, C. H., Zhou, T., et al. (2024). Prediction of soil organic carbon stock combining Sentinel-1 and Sentinel-2 images in the Zoige Plateau, the northeastern Qinghai-Tibet Plateau. *Ecological Processes*, *13*(1), 32. https://doi.org/10.1186/s13717-024-00515-7

Li, C. X., Xu, X. W., Wen, X. Z., Zheng, R. Z., Chen, G. H., Yang, H., et al. (2011). Rupture segmentation and slip partitioning of the mid-eastern part of the Kunlun Fault, north Tibetan Plateau. *Science China Earth Sciences*, *54*(11), 1730–1745. https://doi.org/10.1007/s11430-011-4239-5

Li, Y. F., Henrion, M., Moore, A., Lambot, S., Opfergelt, S., Vanacker, V., et al. (2024). Factors controlling peat soil thickness and carbon storage in temperate peatlands based on UAV high-resolution remote sensing. *Geoderma (Amsterdam)*, *449*, 117009. https://doi.org/10.1016/j.geoderma.2024.117009

Li, Z., He, W., Li, J., Lu, F., & Zhang, H. (2024). Learning without exact guidance: Updating large-scale high-resolution land cover maps from low-resolution historical labels. Paper presented at Proceedings of the IEEE/CVF Conference on Computer Vision and Pattern Recognition. 2024 IEEE/CVF Conference on Computer Vision and Pattern Recognition (CVPR). (pp. 27717–27727). https://doi.org/10.1109/cvpr52733.2024.02618

Li, Z. W., & Gao, P. (2020). Characterizing spatially variable water table depths in a disturbed Zoige peatland watershed. *Journal of Hydro-Environment Research*, *29*, 70–79. https://doi.org/10.1016/j.jher.2020.01.004

Li, Z. W., Gao, P., Hu, X. Y., Yi, Y. J., Pan, B. Z., & You, Y. C. (2020). Coupled impact of decadal precipitation and evapotranspiration on peatland degradation in the Zoige basin, China. *Physical Geography*, *41*(2), 145–168. https://doi.org/10.1080/02723646.2019.1620579

Li, Z. W., Wang, Z. Y., Brierley, G., Nicoll, T., Pan, B. Z., & Li, Y. F. (2015). Shrinkage of the Ruoergai Swamp and changes to landscape connectivity, Qinghai-Tibet Plateau. *Catena (Cremlingen)*, *126*, 155–163. https://doi.org/10.1016/j.catena.2014.10.035

Lilja, H., & Nevalainen, R. (2006). Developing a digital soil map for Finland. In P. Lagacherie, A. B. McBratney, & M. Voltz (Eds.), *Developments in soil science* (pp. 67–74). 603.

Liu, F., Wu, H. Y., Zhao, Y. G., Li, D. C., Yang, J. L., Song, X. D., et al. (2022). Mapping high resolution national soil information grids of China. *Science Bulletin*, *67*(3), 328–340. https://doi.org/10.1016/j.scib.2021.10.013

Liu, Y., Wang, X. Y., Su, Q., Yi, S. W., Miao, X. D., Li, Y. Q., & Lu, H. Y. (2021). Late Quaternary terrace formation from knickpoint propagation in the headwaters of the Yellow River, NE Tibetan Plateau. *Earth Surface Processes and Landforms*, *46*(14), 2788–2806. https://doi.org/10.1002/esp.5208

Lou, X. D., Zhai, S. Q., Kang, B., Hu, Y. L., & Hu, L. L. (2014). Rapid response of hydrological loss of DOC to water table drawdown and warming in Zoige peatland: Results from a Mesocosm experiment. *PLoS One*, *9*(11), e109861. https://doi.org/10.1371/journal.pone.0109861

Luo, L., Zhu, L., Hong, W., Gu, J. D., Shi, D., He, Y., et al. (2021). Microbial resource limitation and regulation of soil carbon cycle in Zoige Plateau peatland soils. *Catena (Cremlingen)*, *205*, 105478. https://doi.org/10.1016/j.catena.2021.105478

Ma, Q. F., Cui, L. J., Song, H. T., Gao, C. J., Hao, Y. Q., Luan, J. W., et al. (2017). Aboveground and belowground biomass relationships in the Zoige peatland, eastern Qinghai-Tibetan plateau. *Wetlands*, *37*(3), 461–469. https://doi.org/10.1007/s13157-017-0882-8

Melton, J. R., Chan, E., Millard, K., Fortier, M., Winton, R. S., Martín-López, J. M., et al. (2022). A map of global peatland extent created using machine learning (Peat-ML). *Geoscientific Model Development*, *15*(12), 4709–4738. https://doi.org/10.5194/gmd-15-4709-2022

Minasny, B., Berglund, Ö., Connolly, J., Hedley, C., de Vries, F., Gimona, A., et al. (2019). Digital mapping of peatlands - A critical review. *Earth-Science Reviews*, *196*, 102870. https://doi.org/10.1016/j.earscirev.2019.05.014

Moore, P. D. (1989). The ecology of peat-forming processes - a review. *International Journal of Coal Geology*, *12*(1–4), 89–103. https://doi.org/10.1016/0166-5162(89)90048-7

National Wetlands Working Group. (1997). *The Canadian wetland classification system* (2nd ed.). Wetlands Research Centre, University of Waterloo.

Parry, L. E., Charman, D. J., & Noades, J. P. W. (2012). A method for modelling peat depth in blanket peatlands. *Soil Use & Management*, *28*(4), 614–624. https://doi.org/10.1111/j.1475-2743.2012.00447.x

Parsekian, A. D., Slater, L., Ntarlagiannis, D., Nolan, J., Sebesteyen, S. D., Kolka, R. K., & Hanson, P. J. (2012). Uncertainty in peat volume and soil carbon estimated using ground-penetrating radar and probing. *Soil Science Society of America Journal*, *76*(5), 1911–1918. https://doi.org/10.2136/sssaj2012.0040

Pezdir, V., Ceru, T., Horn, B., & Gosar, M. (2021). Investigating peatland stratigraphy and development of the Sijec bog (Slovenia) using near-surface geophysical methods. *Catena (Cremlingen)*, *206*, 105484. https://doi.org/10.1016/j.catena.2021.105484

Plado, J., Sibul, I., Mustasaar, M., & Joeleht, A. (2011). Ground-penetrating radar study of the Rahivere peat bog, eastern Estonia. *Estonian Journal of Earth Sciences*, *60*(1), 31–42. https://doi.org/10.3176/earth.2011.1.03

Rampi, L. P., Knight, J. F., & Pelletier, K. C. (2014). Wetland mapping in the upper midwest United States: An object-based approach integrating lidar and imagery data. *Photogrammetric Engineering & Remote Sensing*, *80*(5), 439–448. https://doi.org/10.14358/pers.80.5.439

Rosa, E., Larocque, M., Pellerin, S., Gagné, S., & Fournier, R. (2009). Determining the number of manual measurements required to improve peat thickness estimations by ground penetrating radar. *Earth Surface Processes and Landforms*, *34*(3), 377–383. https://doi.org/10.1002/esp.1741

Rudiyanto, B. M., Setiawan, B. I., Saptomo, S. K., & McBratney, A. B. (2018). Open digital mapping as a cost-effective method for mapping peat thickness and assessing the carbon stock of tropical peatlands. *Geoderma (Amsterdam)*, *313*, 25–40. https://doi.org/10.1016/j.geoderma.2017.10.018

Silvestri, S., Christensen, C. W., Lysdahl, A. O. K., Anschütz, H., Pfaffhuber, A. A., & Viezzoli, A. (2019). Peatland volume mapping over resistive substrates with airborne electromagnetic technology. *Geophysical Research Letters*, *46*(12), 6459–6468. https://doi.org/10.1029/2019gl083025

Slater, L. D., & Reeve, A. (2002). Investigating peatland stratigraphy and hydrogeology using integrated electrical geophysics. *Geophysics*, *67*(2), 365–378. https://doi.org/10.1190/1.1468597

Strack, M., Davidson, S. J., Hirano, T., & Dunn, C. (2022). The potential of peatlands as nature-based climate solutions. *Current Climate Change Reports*, *8*(3), 71–82. https://doi.org/10.1007/s40641-022-00183-9

Sun, J. J., Gallego-Sala, A., & Yu, Z. C. (2023). Topographic and climatic controls of peatland distribution on the Tibetan Plateau. *Scientific Reports*, *13*(1), 14811. https://doi.org/10.1038/s41598-023-39699-x

Tan, Y. C., Wang, Y. F., Chen, Z., Yang, M. Y., Ning, Y., Zheng, C. Y., et al. (2022). Long-term artificial drainage altered the product stoichiometry of denitrification in alpine peatland soil of Qinghai-Tibet Plateau. *Geoderma (Amsterdam)*, *428*, 116206. https://doi.org/10.1016/j.geoderma.2022.116206

Temmink, R. J. M., Robroek, B. J. M., van Dijk, G., Koks, A. H. W., Käärmelahti, S. A., Barthelmes, A., et al. (2023). Wetscapes: Restoring and maintaining peatland landscapes for sustainable futures. *Ambio*, *52*(9), 1519–1528. https://doi.org/10.1007/s13280-023-01875-8

Turetsky, M. R., Kotowska, A., Bubier, J., Dise, N. B., Crill, P., Hornibrook, E. R. C., et al. (2014). A synthesis of methane emissions from 71 northern, temperate, and subtropical wetlands. *Global Change Biology*, *20*(7), 2183–2197. https://doi.org/10.1111/gcb.12580

United Nations Environment Programme. (2022). *Global peatlands assessment: The state of the world's peatlands: Evidence for action toward the conservation, restoration, and sustainable management of peatlands*. UNEP.

Vepraskas, M. J., & Craft, C. B. (2016). *Wetland soils: Genesis, hydrology, landscapes, and classification*. CRC Press.

Wang, M., Chen, H., Wu, N., Peng, C., Zhu, Q., Zhu, D., et al. (2014). Carbon dynamics of peatlands in China during the Holocene. *Quaternary Science Reviews*, *99*, 34–41. https://doi.org/10.1016/j.quascirev.2014.06.004

Wang, M., Yang, G., Gao, Y., Chen, H., Wu, N., Peng, C., et al. (2015). Higher recent peat C accumulation than that during the holocene on the Zoige plateau. *Quaternary Science Reviews*, *114*, 116–125. https://doi.org/10.1016/j.quascirev.2015.01.025

Wittnebel, M., Tiemeyer, B., & Dettmann, U. (2021). Peat and other organic soils under agricultural use in Germany: Properties and challenges for classification. *Mires and Peat*, *27*.

Xu, J. R., Morris, P. J., Liu, J. G., & Holden, J. (2018). PEATMAP: Refining estimates of global peatland distribution based on a meta-analysis. *Catena (Cremlingen)*, *160*, 134–140. https://doi.org/10.1016/j.catena.2017.09.010

Yang, G., Peng, C., Chen, H., Dong, F., Wu, N., Yang, Y., et al. (2017). Qinghai–Tibetan Plateau peatland sustainable. *Ecosystem Health and Sustainability*, *3*(3). https://doi.org/10.1002/ehs2.1263

Young, D. M., Parry, L. E., Lee, D., & Ray, S. (2018). Spatial models with covariates improve estimates of peat depth in blanket peatlands. *PLoS One*, *13*(9), e0202691. https://doi.org/10.1371/journal.pone.0202691

Yu, K.-f., Lehmkuhl, F., & Falk, D. (2017). Quantifying land degradation in the Zoige Basin, NE Tibetan Plateau using satellite remote sensing data. *Journal of Mountain Science*, *14*(1), 77–93. https://doi.org/10.1007/s11629-016-3929-z

Yu, Z. C., Loisel, J., Brosseau, D. P., Beilman, D. W., & Hunt, S. J. (2010). Global peatland dynamics since the last glacial maximum. *Geophysical Research Letters*, *37*(13). https://doi.org/10.1029/2010gl043584

Zhang, G. L., Liu, F., & Song, X. D. (2017). Recent progress and future prospect of digital soil mapping: A review. *Journal of Integrative Agriculture*, *16*(12), 2871–2885. https://doi.org/10.1016/s2095-3119(17)61762-3

Zhang, H. T., Wang, J., Zhang, Y., Qian, H., Xie, Z., Hu, Y., et al. (2023). Soil organic carbon dynamics and influencing factors in the Zoige alpine wetland from the 1980s to 2020 based on a random forest model. *Land*, *12*(10), 1923. https://doi.org/10.3390/land12101923